AGU ADVANCING EARTH AND SPACE SCIENCE

Geophysical Research Letters

RESEARCH LETTER
10.1029/2021GL092378

Observed Trends in the South Asian Monsoon Low-Pressure Systems and Rainfall Extremes Since the Late 1970s

Yujia You[1,2] **and Mingfang Ting**[1]

[1]Lamont-Doherty Earth Observatory, Columbia University, Palisades, NY, USA, [2]Department of Earth and Environmental Sciences, Columbia University, New York, NY, USA

Key Points:

- An extreme rainfall dipole with positive trends over south-central India and negative trends over north-central India is observed since 1979
- The extreme rainfall dipole aligns with the trends in the number of Indian monsoon low-pressure systems passing through the two regions
- The changing LPS translation is likely associated with a wetter environment owing to a strengthened cross-equatorial moisture transport

Supporting Information:

Supporting Information may be found in the online version of this article.

Correspondence to:

Y. You,
yujia@ldeo.columbia.edu

Citation:

You, Y., & Ting, M. (2021). Observed trends in the South Asian monsoon low-pressure systems and rainfall extremes since the late 1970s. *Geophysical Research Letters*, *48*, e2021GL092378. https://doi.org/10.1029/2021GL092378

Received 2 JAN 2021
Accepted 7 APR 2021

Abstract The core Indian monsoon region receives more than half of the rainfall extremes from low-pressure systems (LPSs), which typically form over the Bay of Bengal and propagate upstream against the time-mean low-level westerlies. Yet, the relationship between the trends of LPSs and rainfall extremes remains uncertain. Using two tracking algorithms and reanalyses-derived LPSs, we find that LPS activity and extreme rainfall exhibit coherent trends during the post-1979 satellite era. Over time, the LPSs propagate preferentially into south-central India rather than north-central India, imparting a corresponding dipole footprint in rainfall extremes. Consistent with existing theories that the diabatic heating is instrumental in shifting the LPSs west-southwestward, the LPSs traveling through south-central India have stronger updrafts on their west-southwestern flank than those passing through north-central India. The increased frequency of LPSs propagating into south-central India is likely due to a strengthened cross-equatorial moisture transport, which favors stronger storm ascents.

Plain Language Summary The South Asian synoptic-scale low-pressure systems (LPSs), which typically form over the Bay of Bengal and propagate upstream against the time-mean low-level westerlies, produce more than half of the summer rainfall extremes over the densely populated central India. Given the vulnerability of societies in this region to rainfall extremes, investigating the connection between LPSs and extreme rainfall regarding their long-term trends has important implications for climate adaptation. Using two different tracking algorithms and reanalyses-derived LPS tracks, we find that the trends of extreme rainfall and LPS activity exhibit a strong coherence during the post-1979 satellite era. Specifically, the LPSs prefer to propagate into south-central India than north-central India over time, imparting a corresponding dipole footprint in rainfall extremes. In agreement with previous studies that the LPS propagation is a combined effect of the northwestward-propagating component due to horizontal nonlinear adiabatic advection and the southwestward-propagating component due to diabatic heating, we notice that the LPSs migrating through the south-central India have stronger updrafts on their west-southwestern flank compared to those passing through north-central India. Our results indicate that the increasing number of LPSs propagating into south-central India is likely due to a strengthened cross-equatorial moisture transport, which provides a wetter environment and favors stronger storm ascents.

1. Introduction

South Asia, one of the most densely populated regions in the world, receives more than 80% of annual rainfall during the summer monsoon season (June–September, JJAS), when the monsoonal southwesterlies transport abundant moisture from the tropical Indian Ocean into the subcontinent (e.g., Malik et al., 2016). While agricultural yield and water resources in this region benefit from the monsoon rainfall, human lives and infrastructures are, at the same time, threatened by the frequently occurring heavy downpour. Over India, extreme rainfall is closely tied to the synoptic-scale low-pressure systems (LPSs), which occur frequently during the monsoon season with an average number of about 13 (±3) storms each summer (Krishnamurthy & Ajaymohan, 2010; Praveen et al., 2015; Sikka, 1977). The Indian monsoon LPSs typically form over the Bay of Bengal (BoB) and adjacent land, having a horizontal length scale of about 1,000–2,000 km, propagating west-northwestward across central India, and terminating over northwestern India (e.g., Hunt et al., 2016; Krishnamurthy & Ajaymohan, 2010). Indian LPSs are often categorized into monsoon lows, monsoon depressions, and deep depressions based on the maximum sustained surface wind speed (i.e.,

8.5–13.4 m/s for monsoon depressions, weaker for monsoon lows, and stronger for deep depressions). Even though the Indian LPSs are typically weaker than tropical cyclones, they often initiate intense rainfall over the west-southwest flank of the storm centers (Mooley, 1973; Yoon & Chen, 2005).

Fractionally, the Indian monsoon LPSs account for more than half of the Indian summer rainfall totals and extremes (e.g., Hunt & Fletcher, 2019; Hurley & Boos, 2015). Given the predominance of monsoon LPSs in shaping the Indian extreme rainfall, exploring the physical processes behind the long-term trend of LPS activity and identifying the role of changing LPS activity in modulating the rainfall extremes have potentially important implications for disaster risk management and future climate adaptation. Although this topic has garnered a great deal of interest in the literature, the connections between the trends of LPS and extreme rainfall remain elusive. Based on the manually compiled LPS tracks provided by the Indian Meteorological Department (IMD), earlier studies have reported a downward trend in the occurrence of depression-strength LPSs during the mid-20th to the early 21st centuries (e.g., Prajeesh et al., 2013; Vishnu et al., 2016). However, this declining trend is opposite to the increasing trend of the very intense rainfall events over central India as derived from the IMD gridded gauge observations (e.g., Goswami et al., 2006; Pai et al., 2014; Rajeevan et al., 2008; Roxy et al., 2017). Ajayamohan et al. (2010) reconciled this contradiction by showing that the declining occurrence of depressions is overweighed by a rising occurrence of low-strength LPSs, while others have proposed alternative mechanisms to explain the extreme rainfall trend, such as urbanization (Shastri et al., 2015), tropical Indian Ocean warming (Goswami et al., 2006), enhanced variability of the low-level monsoon westerlies over the Arabian Sea (Roxy et al., 2017), and increased dew point temperature due to anthropogenic forcings (Mukherjee et al., 2018). Yet, the conflicting trends of monsoon depression activity and rainfall extremes may be caused by uncertainties in the IMD LPS and rainfall records. For example, Cohen and Boos (2014) and Vishnu et al. (2020) identified several depression-strength LPSs in satellite measurements during the years when IMD recorded none. They also showed that no detectable trend can be identified in either monsoon depressions or monsoon lows according to reanalysis-based LPS tracks. Lin and Huybers (2019), on the other hand, pointed out that one of the greatest uncertainties in estimating the Indian extreme rainfall trend comes from the temporal variations in the rain-gauge network, which artificially enhanced rainfall extremes over central India after the 1970s (see also Singh et al., 2019).

These conflicting results call for a revisit of the Indian LPS–extreme rainfall relationship, especially in terms of their secular trends. In the present study, specific questions we seek to address include the following. How have the Indian monsoon LPSs and extreme rainfall changed in the recent past? To what extent is the trend in rainfall extremes accounted for by changing LPS activity and what are the physical mechanisms underlying the trends? As possible errors in the IMD LPS records make observed LPS tracks less ideal for trend analysis (Cohen & Boos, 2014; Vishnu et al., 2020), in the present study we pursue these questions and test the robustness of our findings by utilizing reanalysis products and two independent tracking algorithms to identify monsoon LPSs (includes monsoon lows, depressions, and deep depressions). The agreement between the two tracking methods can provide confidence for the robustness of our conclusions. Considering the time period covered by reanalysis products, here we focus on the post-1979 satellite era spanning from 1979 to 2018.

2. Data and Method

Owing to the overall weaker intensity of Indian monsoon LPSs as compared to tropical cyclones, tracking LPSs using reanalysis poses some challenges to the tracking algorithms. Previous studies have attempted to track monsoon LPSs in various reanalysis products and model outputs (e.g., Hurley & Boos, 2015; Praveen et al., 2015; Sandeep et al., 2018; Vishnu et al., 2020; You & Ting, 2021). Here, we follow the tracking procedure discussed in You and Ting (2021) and You et al. (2021) but employ two different tracking algorithms, that is, TempestExtremes (Ullrich & Zarzychi, 2017) and TRACK (K. I. Hodges, 1994, 1995, 1999), to objectively track the JJAS Indian monsoon LPSs using the 6-hourly European Centre for Medium-Range Weather Forecasts Interim Re-Analysis spanning 1979–2018 (ERA-I; Dee et al., 2011). Both algorithms have been applied extensively to track tropical and extratropical cyclones (e.g., K. Hodges et al., 2017; Zarzycki & Ullrich, 2017). The details of the tracking algorithms are provided in supplementary Text S1. Briefly, the tracking algorithms identify and track 850 hPa relative vorticity local maxima exceeding 5×10^{-6} s^{-1} at each

time step. The vorticity field is first spectrally filtered to retain total wavenumber 5–42 to emphasize the synoptic-scale disturbances. The initial tracks are produced by connecting vorticity maxima at sequential time steps. Among the identified tracks, only those accompanied by a minimum in sea level pressure anomaly relative to the 21-day running mean, lasting at least 3 days, and having no less than one track point within the domain 15°N–30°N, 75°E–90°E are retained. To evaluate the robustness of our conclusions, we verify our results using the LPS tracks constructed by Vishnu et al. (2020), which are available for five reanalysis products. Although Vishnu et al. (2020) also employed TempestExtremes, they detected LPSs based on the 850 hPa stream function.

To measure LPS activities, the genesis density, track density, and translation velocity are calculated. The genesis (track) density indicates the frequency of LPSs that form near (pass through) a grid point and is computed by counting the number of LPS genesis (track) points within 500 km of each grid point each summer from June to September. Because the LPS locations are reported at 6-hourly intervals, we further divide the track density by four to convert the unit into number of LPS days. The translation velocity is computed using neighboring track positions. To identify LPS-related rainfall, the gridded daily rainfall at $0.25° \times 0.25°$ resolution for the period 1979–2018 is taken from IMD, which contains the highest number of stations than any gridded data sets currently available (Pai et al., 2014). To reduce the uncertainty arising from internal noises, rainfall at each grid point is smoothed by pooling data from eight neighboring grid cells before any analysis is performed (Figure S1). The ERA-I winds, precipitable water, and temperature are used to associate the synoptic LPS activity with the large-scale environment.

The trends of extreme precipitation and LPS activity are estimated through linear regressions, of which the significance is tested by a nonparametric Mann–Kendall test (Kendall, 1975; Mann, 1945). As the number of LPSs passing through a certain area is determined by multiple factors (i.e., genesis location, genesis frequency, and propagation pathway) that are governed by very different physical processes, we adopt a decomposition method to attribute the trend (e.g., Yokoi et al., 2013; You & Ting, 2021). Specifically, the total number of LPSs passing through an area A [$N(A)$] in a given time period can be expressed as

$$N(A) = \iint G(A_0)P(A,A_0)\mathrm{d}A_0 \tag{1}$$

where $G(A_0)$ denotes the total number of LPSs formed at grid point A_0. $P(A,A_0)$ is the probability for LPSs formed at A_0 to propagate into A, which ranges from 0 to 1. $N(A)$ is therefore the spatial integration of the product of $G(A_0)$ and $P(A,A_0)$ over all grid points in which LPSs form. The difference of $N(A)$ between two time periods [$\Delta N(A)$] can be partitioned into

$$\Delta N(A) = \iint \Delta G(A_0)P(A,A_0)\mathrm{d}A_0 + \iint G(A_0)\Delta P(A,A_0)\mathrm{d}A_0 + \iint \Delta G(A_0)\Delta P(A,A_0)\mathrm{d}A_0 \tag{2}$$

in which the three terms on the right-hand side represent the changes due to genesis, propagation, and a nonlinear effect, respectively. Each of the three terms is further normalized by dividing by $\Delta N(A)$ to obtain the normalized contributions.

3. Results

3.1. Association Between Extreme Rainfall and LPS Activity

To measure LPS activity, Figure 1 presents the climatologies of LPS genesis density, translation vectors, and track density based on the LPS trajectories compiled by the two tracking algorithms. Both algorithms provide a realistic representation of LPS activity as compared to the manually tracked records (Praveen et al., 2015). The TempestExtremes and TRACK detect approximately 10.0 and 10.7 LPSs each summer, respectively. The LPSs form most frequently over the BoB and adjoining land, migrating northwestward across central India (Figures 1a, 1b, 1d, and 1e). Note that while the LPS track densities derived from TempestExtremes and TRACK feature a similar climatological pattern, the magnitude of the former is smaller than the latter with the most significant difference near the BoB and adjoining land (compare the contours in Figures 1b and 1e). Since the two algorithms capture a similar number of LPSs, this suggests that on average either the translation speed of the TRACK-derived LPSs is slower or the LPSs detected by TRACK are more inclined to pass through the BoB. The former possibility is supported by the climatological translation vectors displayed in Figures 1a and 1d. The latter turns out to be valid since the maximum genesis density

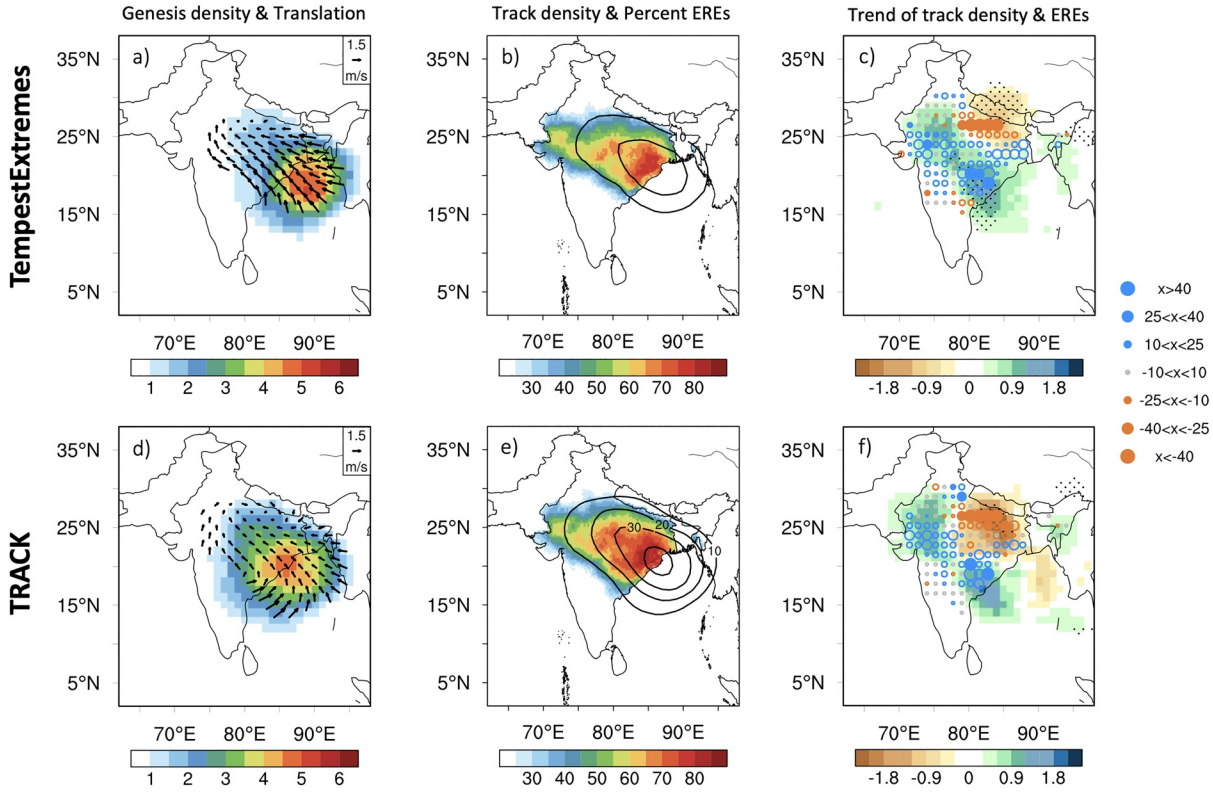

Figure 1. Climatology and trend of JJAS LPS activity based on (top) TempestExtremes and (bottom) TRACK during period 1979–2018. (a, d) Climatological LPS genesis density (number of LPSs per summer; shading) and translation velocity (m/s; vector). (b, e) Climatological LPS track density (number of LPS days per summer; contour) and fractional contribution to rainfall extremes (%; shading). (c, f) Trend of LPS track density (number of LPS days per decade; shading) and LPS-related extreme daily rainfall amount (mm/decade; dot). The extreme daily rainfall is defined as exceedances of the 90th percentile of the JJAS daily rainfall. JJAS, June–September; LPS, low-pressure system.

of the TRACK-derived LPSs already straddles the BoB as compared to that of the TempestExtremes (Figures 1a and 1d). This discrepancy does not affect our conclusions and the two tracking algorithms agree on the temporal changes in LPS activities, as will be shown later.

Besides the spatial patterns of the genesis and track density, the LPSs captured by the two exhibit a consistent structure agreeing with observations, that is, the LPSs have the strongest amplitude in the lower troposphere, and the most intense rainfall occurs to the west and southwest of the cyclone center within the 500 km radius (Figure S2; Hunt et al., 2016). Consequently, we consider daily rainfall to be LPS induced when a LPS is within 500-km radius of the grid point during a time window of ±1 day. The time window of ±1 day is to accommodate the potential underestimation due to the rainfall daily resolution, as the precipitation from a single storm occurs within a consecutive time window and may run across midnight from one day to the next (e.g., Khouakhi et al., 2017; Knight & Davis, 2009). To avoid double counting, every rainfall event is counted only once.

To what extent do the LPSs contribute to rainfall extremes and how has the LPS activity changed in the recent 40-year period? Adopting the peak-over-threshold method, here we define extreme daily rainfall at each grid point as exceedances of the 90th percentile of JJAS daily rainfall (Figure S3). This threshold can be interpreted as 1-in-10-year recurrence interval, which gives 488 extreme events per grid point. As depicted in Figures 1b and 1e, the LPS-related extreme rainfall accounts for more than half of the rainfall extremes over central India. For both tracking algorithms, the trends of LPS track density and its footprint on rainfall extremes exhibit a coherent dipole pattern with decreasing extremes over north-central India near the foothills of the Himalayas and increasing extremes across northwest and south-central India. We focus on the increasing rainfall in south-central India and decreasing rainfall in north-central India as these two regions are located near the core monsoon region, where the most intense rainfall occurs (Figure S3).

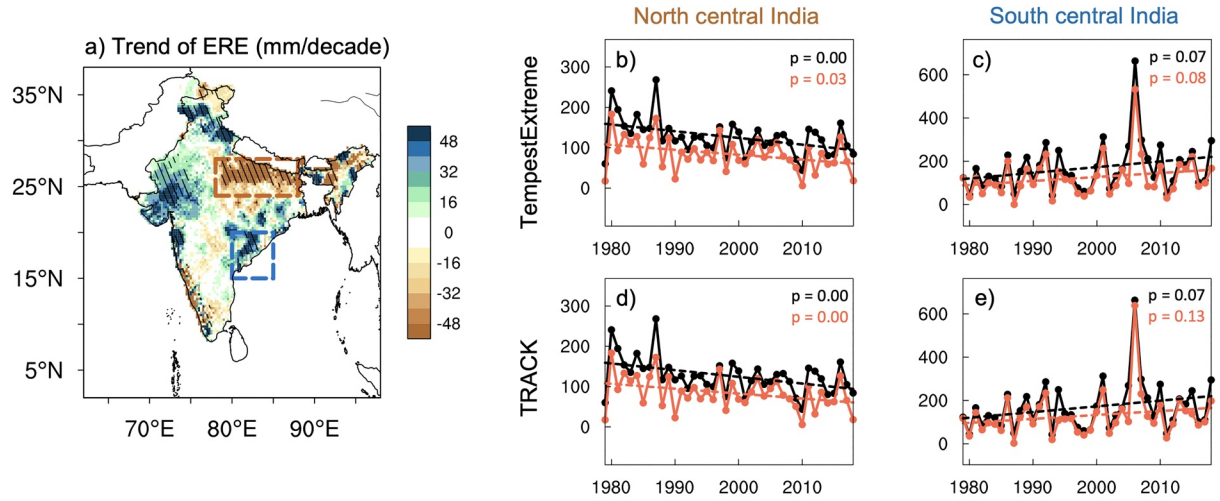

Figure 2. (a) Linear trend of the extreme daily rainfall summed over each summer season (mm/decade). The extreme daily rainfall here is defined as exceedances of the 90th percentile of the JJAS daily rainfall. The hatching indicates statistical significance at the 90% confidence level or above. (b) Time series and linear trend of the total (black line) and LPS-related (red line) extreme rainfall over (b, d) the brown (24°N–28°N and 78°E–88°E) and (c, e) the blue (15°N–20°N, 80°E–85°E) boxed areas in (a). (b, c) For TempestExtremes and (d, e) for TRACK. JJAS, June–September; LPS, low-pressure system.

The dipole pattern suggests that more (fewer) LPSs pass through the south (north) central India in recent years. The robustness of the track density dipole is verified using the LPS track archives compiled by Vishnu et al. (2020) (Figure S4).

Does the changing LPS track density have significant consequences for the total extreme rainfall? The linear trend of extreme daily rainfall summed over each monsoon season reveals a dipole pattern coinciding well with the changes in LPS track density (Figure 2a). After disaggregating the total extreme rainfall trend into components due to changes in frequency and changes in intensity, the dipole is essentially the result of changing extreme rainfall frequency, in line with the LPS track density dipole (Text S3; Figure S5). Furthermore, the time series of total and LPS-related extreme rainfall amounts in the two regions show a high degree of agreement (Figures 2b–2e). Altogether, the above findings indicate that the change in LPS activity is the predominant factor in explaining the dipole pattern of rainfall extremes. The increased extremes over westernmost India are not discussed in the present study as it is located near the arid and semiarid regions where few LPSs pass through.

Compared to the high thresholds used by earlier works to define rainfall extremes (e.g., 99th percentile as in Goswami et al. [2006]; 150 mm/day as in Roxy et al. [2017]), here the 90th percentile threshold is comparatively moderate. In view of this, we calculate the linear trend by percentile bins for the two boxed regions that exhibit the most pronounced trends (Figure S6). Because the daily rainfall distribution is highly skewed toward light and moderate rain events, we divide the rainfall distribution into nine logarithmically spaced bins following G. Chen et al. (2019) (Text S2). In both regions, the daily rainfall at top percentiles shows consistent trends, whereas the weak rainfall tends to vary in an opposite direction. One caveat pertinent to the dipole trend patterns is the artificial extreme rainfall trend introduced by the time-varying rain-gauge networks, as pointed out by Lin and Huybers (2019). We thus repeat the trend calculation using the relatively coarser IMD 1° × 1° gridded rainfall product, which has comparatively moderate temporal changes in station numbers compared to the IMD 0.25° × 0.25° gridded rainfall shown in Figures 1 and 2 (Figure S7; Singh, 2019). We also compare the time series of rainfall extremes over the two boxed regions using the longest temporal coverage of two satellite-based gridded rainfall data sets (late 1990s–2018; TRMM and GPCP1DD) (Figure S8), all show consistent trends as seen in Figure 2.

3.2. Physical Mechanisms Driving the Changes in LPS Track Density

To assess the relative importance of LPS genesis and propagation in driving the LPS track density dipole in Figures 1c and 1g, the decomposition method discussed in Equation 2 is applied to the epoch changes of

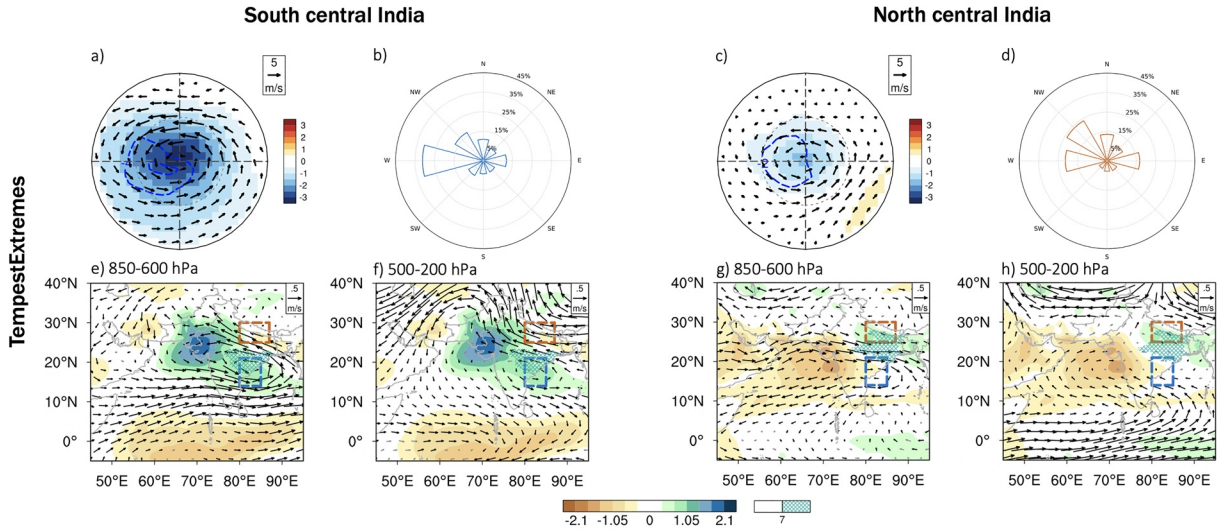

Figure 3. Differences in (first row) the synoptic-scale flow and (second row) the slowly evolving environments between LPSs that form over the BoB and propagate through (left panel) south-central India and (right panel) north-central India. (a, c) LPS-centered composites of 21-day high-passed sea level pressure (hPa; shading), 850 hPa wind (m/s; vector), and vertical velocity (10^{-2} Pa/s; contour) anomalies. (b, d) Percent frequency of LPS translation directions. Geographically fixed composites of the 21-day low-passed wind averaged over (e, g) 850–600 hPa and (f, h) 500–200 hPa (m/s; vectors), overlapped with 21-day low-passed total column water vapor (kg/m^2; shading) and the LPS-related daily rainfall (mm/day; blue hatching). The blue and brown colors used in (b) and (d) are used to indicate the LPSs passing the south-central India (blue boxes in (e)–(h)) and north-central India (brown boxes in (e)–(h)), respectively. LPS, low-pressure system; BoB, Bay of Bengal.

$N(A)$ over the two dipole centers (i.e., 1999–2018 minus 1979–1998). The normalized contributions of the genesis and propagation terms and their spatial distributions are presented in Figure S9. In both regions, the changes in LPS tracks dominate (Figures S8a and S8d), and the changes in tracks are primarily associated with the LPSs formed over the BoB (15°N–25°N, 80°E–95°E; Figures S8b, S8c, S8e, and S8f). This indicates that the LPSs formed over BoB propagate preferentially to the south center rather than the north center in the study period, leading to the track density dipole trend. The contribution from changes in genesis is negligible. This conclusion is further verified by the time series of LPS numbers that formed over BoB and propagate into the two dipole centers (Figure S10).

Determining the causes for the changes in the Indian LPS tracks is challenging because the Indian LPSs propagate northwestward against the time-mean low-level westerlies, and because the upper-level easterlies have little effect on LPS propagation as the vertical extent of the LPS is restricted by the Tibetan anticyclone at around 300 hPa (Yoon & Chen, 2005). Although there is no clear consensus regarding the propagation mechanism of Indian LPSs, it is generally agreed that the propagation is mainly controlled by nonlinear self-advection processes rather than the linear advection by mean flow, and the diabatic heating is instrumental in shifting the LPSs west-southwestward (e.g., Boos et al., 2015, 2017; T.-C. Chen et al., 2005). Specifically, T.-C. Chen et al. (2005) argued that the vertical ascents to the west-southwest of the LPS center (Figures S2c and S2f) induce a strong vortex stretching, causing the vortex to propagate west-southwestward. While Boos et al. (2015, 2017) argued that the vortex stretching is balanced by other terms in vorticity budget and is thus unable to explain the upstream propagation, they suggested that the propagation of LPSs is a combined effect of the northwestward-propagating component due to horizontal nonlinear adiabatic advection and the southwestward-propagating component due to diabatic heating and vertical advective tendencies.

Based on these theories, to evaluate the role of the synoptic-scale LPS circulation and the slowly evolving larger-scale environment in modulating LPS propagation, we assess the storm-centered composites of synoptic-scale flow and examine the geographically fixed composites of large-scale atmospheric environments for LPSs formed over BoB and passing through the north or south dipole center (Figure 3). Considering the periodicity of the intraseasonal modes of Indian summer monsoon (e.g., Krishnamurthy & Shukla, 2007), the synoptic-scale flows (large-scale environments) are obtained from daily anomalies by

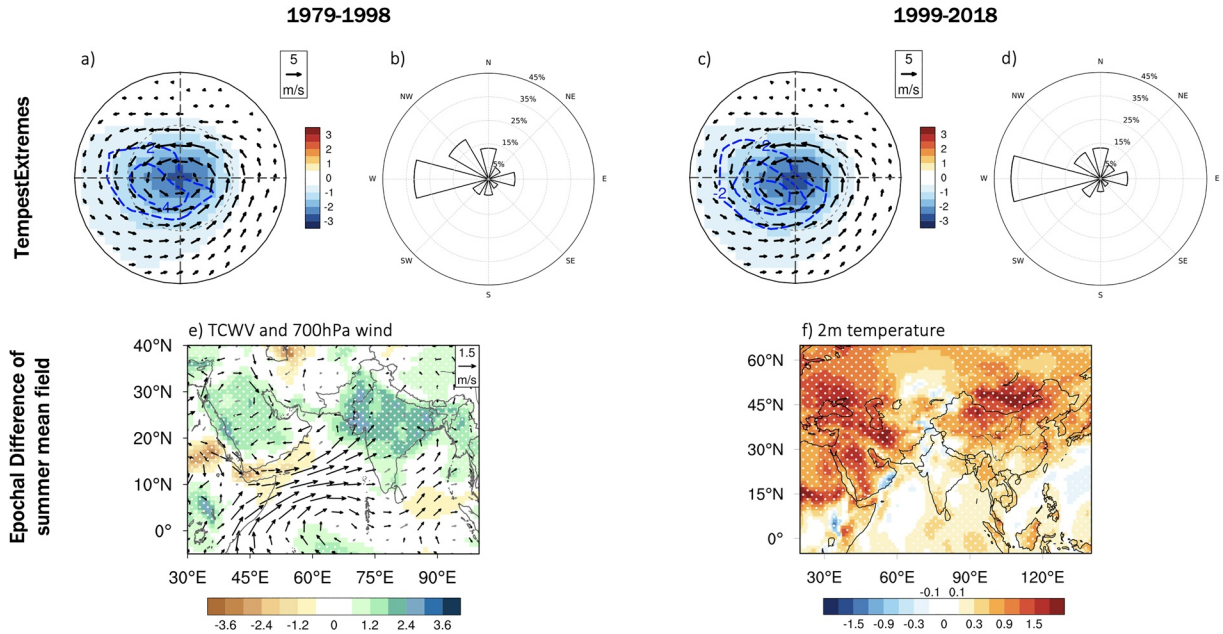

Figure 4. (top) Epochal changes in LPS structure and mean summer environments. (a, c) LPS-centered composites of the 21-day high-passed sea level pressure (hPa; shading), 850 hPa wind (m/s; vector), and vertical velocity (10^{-2} Pa/s; contour), (b, d) Percent fraction of LPS translation direction over period (left) 1979–1998 and (right) 1999–2018 based on TempestExtreme LPSs. (bottom) Epochal differences of the mean summer (e) 700 hPa wind (m/s; vector), precipitable water (kg/m^2; shading), and (f) 2-m air temperature (K; shading). White stippling and black vectors indicate statistical significance at the 90% confidence level or above based on a two-tailed Student's *t* test. LPS, low-pressure system.

applying a high-pass (low-pass) filter with a cutoff period of 21 days. The first row of Figure 3 exhibits the LPS-centered composites of synoptic-scale fields, as well as the percent frequency of LPS translation direction based on TempestExtreme tracks. Consistent with the aforementioned theories, the LPSs propagating through the south center have a more pronounced westward-propagating component (left panel), which is linked to the stronger updraft in their west-southwest quadrant, as compared to the LPSs passing through the north center (right panel). The second row of Figure 3 presents the composites of large-scale environments during LPS active days, which are represented by the low-pass-filtered winds and precipitable water. For LPSs passing through the southern center (left panels), the enhanced low-level southwesterlies bring moisture into the Indian subcontinent and an anomalous cyclone is prevalent over central India, resembling the atmospheric conditions during active spells (Pai et al., 2016). The ample moisture supply provides a favorable condition for more intense updrafts via the conditional instability of the second kind (CISK) mechanism, therefore adding a stronger west-southwestward component to the translation vectors (Figure 3b). For LPSs traveling through the northern center (right panels), the anomalous anticyclone over the northern Arabian Sea suppresses the cross-equatorial moisture transport, and the anomalous westerlies on the poleward flank of the anticyclone bring relatively dry air from the deserts, making the environment unfavorable for storm ascents and strong convection. Consequently, the translation vectors have a (weaker) larger (west-southwestward) north-northwestward propagating component (Figure 3d), consistent with the propagation theory proposed by Boos et al. (2015, 2017). Results based on TRACK algorithm are similar (Figure S11).

With the propagation mechanisms determined, we now compare the epochal difference of the LPS composite structure (Figure 4, first row). Consistent with the dipole pattern, the LPSs derived by TempestExtremes become stronger in the later period, and the intensified ascent southwest of the vortex center boosts the west-southwestward propagation (compare left and right panels). Similar results are obtained based on TRACK algorithm (Figure S12). The intensification of LPSs in the later period is possibly attributed to the significantly enhanced seasonal-mean monsoonal southwesterlies. The anomalous moisture transport leads to an increase in precipitable water over the Indian subcontinent (Figure 4e), which is favorable for enhanced LPS updrafts. The contribution of local surface moisture fluxes from the Indus and the Ganges

River Valley is minor according to a moisture budget analysis (not shown). The strengthened seasonal-mean monsoon circulation is possibly driven by the stronger land–sea thermal gradient due to the significant warming over the Eurasian landmass (Figure 4f), which resembles the "warm ocean-warmer land" effect as proposed by previous studies (Lau et al., 2017). A similar pattern of epochal difference can be found in the near-surface moist static energy (MSE) field, which reinforces the climatological MSE meridional gradients and thus leads to a more intense monsoon circulation (Figure S13).

4. Summary and Discussion

Using reanalysis-based Indian LPS trajectories compiled by two tracking algorithms and IMD gauge-based daily rainfall observations, we found that over the period 1979–2018, the secular variation of rainfall extremes over India is characterized by a dipole-like pattern with increased rainfall extremes over south-central India and decreased rainfall extremes over north-central India. The dipole trend pattern is mainly driven by the changes in extreme rainfall frequency and is spatially coherent with the changes in LPS exposure, that is, more (less) LPSs tend to travel through the south (north) central India over time. LPS propagation was identified to be the main factor responsible for the changes in the number of LPS passing through the two areas, whereas the changes in LPS genesis make only minor contributions.

In contrast to the tropical cyclone motion which is mainly governed by steering flow, the Indian LPSs typically propagate northwestward against the time-mean monsoonal westerlies in the lower troposphere where the LPSs show the peak intensity. Hence, the large-scale steering concept does not apply to Indian LPSs. Conversely, the Indian LPS motion is primarily controlled by nonlinear self-advection processes, in which the diabatic heating plays an important role in shifting the LPS west-southwestward and the horizontal nonlinear adiabatic advection drives the LPSs northwestward (Boos et al., 2015, 2017; T.-C. Chen et al., 2005). Consistent with the propagation theory, our results suggest that compared to the LPSs propagation into north-central India, the LPSs passing through south-central India exhibit significantly stronger ascents over the west-southwestern quadrant, likely due to the anomalously wet environments these storms are embedded in and hence the more effective CISK mechanism. During the study period, the mean summer cross-equatorial flow along the Somali coast has strengthened over time, enhancing the moisture transport toward the Indian subcontinent. The increase in moisture content provides an environment favorable for stronger convection and more intense storms, thus promoting the west-southwestward propagation of LPSs. We note that while the intensity of LPS increases during the period, the increase only makes a minor contribution and the dipole trend pattern of extreme rainfall is primarily ascribed to the changes in LPS track density.

Although identifying the historical relationship between extreme rainfall trend and LPS activity has important implications toward understanding the regional impact of anthropogenic forcings, advances on such topic were hindered by the potential errors in the manually compiled LPS records and by the caveats related to the gridded daily rainfall data set (Cohen & Boos, 2014; Lin & Huybers, 2019; Singh et al., 2019; Vishnu et al., 2020). Here, we employed two independent tracking algorithms for the robustness of the LPS tracking, and the agreement among different reanalyses boosts confidence in the robustness of our findings (Figures 1 and S4). We speculate that the impact of anthropogenic greenhouse gas forcing is implied by the significantly strengthened summer-mean monsoon circulation, which is likely relevant to the considerable warming over Eurasian landmass and hence the enhanced land–sea thermal contrast (Figure 4). The strengthening of the Indian monsoon is opposite to those found in previous studies, which reported a weakening in the period 1950s–2000s (Annamalai et al. 2013; Roxy et al., 2015; Vishnu et al., 2016). Probable causes behind such discrepancies involve both the positive to the negative phase transition of the Pacific Decadal Oscillation near the late 1990s, which favors stronger monsoon flow (Krishnamurthy & Krishnamurthy, 2014), and the aerosol forcing which masks greenhouse-warming-induced changes in the earlier period (e.g., Lau et al., 2017; Li et al., 2015). Consequently, further modeling studies are needed to ascertain whether the extreme rainfall and LPS trends are a result of anthropogenic external forcing or internal climate variability.

Data Availability Statement

Data associated with this study are publicly available in their existing repositories for Indian Meteorology Department (https://www.imdpune.gov.in/Clim_Pred_LRF_New/Grided_Data_Download.html) and ERA-Interim (https://www.ecmwf.int/en/forecasts/datasets/reanalysis-datasets/era-interim). The two tracking algorithms can be found online at https://github.com/ClimateGlobalChange/tempestextremes for TempestExtremes and http://www.nerc-essc.ac.uk/~kih/TRACK/Track.html for TRACK. The Indian LPS tracks compiled for this study can be found at Zenodo repository (https://doi.org/10.5281/zenodo.4306771).

Acknowledgments
This research was supported by the National Science Foundation grant AGS16-07348. Y. You. was supported by National Aeronautics and Space Administration (NASA) under the Future Investigators in NASA Earth and Space Science and Technology (FINESST) program—grant 19-EARTH20-0243.

References

Ajayamohan, R. S., Merryfield, W. J., & Kharin, V. V. (2010). Increasing trend of synoptic activity and its relationship with extreme rain events over central India. *Journal of Climate*, *23*, 1004–1013. https://doi.org/10.1175/2009JCLI2918.1

Annamalai, H., Hafner, J., Sooraj, K. P., & Pillai, P. (2013). Global warming shifts the monsoon circulation, drying South Asia. *Journal of Climate*, *26*(9), 2701–2718. https://doi.org/10.1175/JCLI-D-12-00208.1

Boos, W. R., Hurley, J. V., & Murthy, V. S. (2015). Adiabatic westward drift of Indian monsoon depressions. *Quarterly Journal of the Royal Meteorological Society*, *141*, 1035–1048. https://doi.org/10.1002/qj.2454

Boos, W. R., Mapes, B. E., & Murthy, V. S. (2017). Potential vorticity structure and propagation mechanism of Indian monsoon depressions. In C.-P. Chang, H.-C. Kuo, N.-C. Lau, R. H. Johnson, B. Wang, & M. C. Wheeler (Eds.), *World scientific series on Asia-Pacific weather and climate. The global monsoon system*. Singapore: World Scientific.

Chen, G., Norris, J., Neelin, J. D., Lu, J., Leung, L. R., & Sakaguchi, K. (2019). Thermodynamic and dynamic mechanisms for hydrological cycle intensification over the full probability distribution of precipitation events. *Journal of the Atmospheric Sciences*, *76*, 497–516. https://doi.org/10.1175/JAS-D-18-0067.1

Chen, T.-C., Yoon, J.-H., & Wang, S.-Y. (2005). Westward propagation of the Indian monsoon depression. *Tellus A*, *57*, 758–769. https://doi.org/10.3402/tellusa.v57i5.14733

Cohen, N. Y., & Boos, W. R. (2014). Has the number of Indian summer monsoon depressions decreased over the last 30 years? *Geophysical Research Letters*, *41*, 7846–7853. https://doi.org/10.1002/2014GL061895

Dee, D. P., Uppala, S. M., Simmons, A. J., Berrisford, P., Poli, P., Kobayashi, S., et al. (2011). The ERA-Interim reanalysis: Configuration and performance of the data assimilation system. *Quarterly Journal of the Royal Meteorological Society*, *137*, 553–597. https://doi.org/10.1002/qj.828

Goswami, B. N., Venugopal, V., Sengupta, D., Madhusoodanan, M. S., & Xavier, P. K. (2006). Increasing trend of extreme rain events over India in a warming environment. *Science*, *314*, 1442–1445.

Hodges, K., Cobb, A., & Vidale, P. L. (2017). How well are tropical cyclones represented in reanalysis datasets? *Journal of Climate*, *30*, 5243–5264. https://doi.org/10.1175/JCLI-D-16-0557.1

Hodges, K. I. (1994). A general method for tracking analysis and its application to meteorological data. *Monthly Weather Review*, *122*, 2573–2586. https://doi.org/10.1175/1520-0493(1994)122<2573:AGMFTA>2.0.CO;2

Hodges, K. I. (1995). Feature tracking on the unit sphere. *Monthly Weather Review*, *123*, 3458–3465. https://doi.org/10.1175/1520-0493(1995)123<3458:FTOTUS>2.0.CO;2

Hodges, K. I. (1999). Adaptive constraints for feature tracking. *Monthly Weather Review*, *127*, 1362–1373. https://doi.org/10.1175/1520-0493(1999)127<1362:ACFFT>2.0.CO;2

Hunt, K. M. R., & Fletcher, J. K. (2019). The relationship between Indian monsoon rainfall and low-pressure systems. *Climate Dynamics*, *53*, 1859–1871. https://doi.org/10.1007/s00382-019-04744-x

Hunt, K. M. R., Turner, A. G., Inness, P. M., Parker, D. E., & Levine, R. C. (2016). On the structure and dynamics of Indian monsoon depressions. *Monthly Weather Review*, *144*, 3391–3416. https://doi.org/10.1175/MWR-D-15-0138.1

Hurley, J. V., & Boos, W. R. (2015). A global climatology of monsoon low-pressure systems. *Quarterly Journal of the Royal Meteorological Society*, *141*, 1049–1064. https://doi.org/10.1002/qj.2447

Kendall, M. G. (1975). *Rank correlation measures* (202 pp.). London: Charles Griffin.

Khouakhi, A., Villarini, G., & Vecchi, G. A. (2017). Contribution of tropical cyclones to rainfall at the global scale. *Journal of Climate*, *30*, 359–372. https://doi.org/10.1175/JCLI-D-16-0298.1

Knight, D. B., & Davis, R. E. (2009). Contribution of tropical cyclones to extreme rainfall events in the southeastern United States. *Journal of Geophysical Research*, *114*, D23102. https://doi.org/10.1029/2009JD012511

Krishnamurthy, L., & Krishnamurthy, V. (2014). Influence of PDO on South Asian summer monsoon and monsoon-ENSO relation. *Climate Dynamics*, *42*(9–10), 2397–2410. https://doi.org/10.1007/s00382-013-1856-z

Krishnamurthy, V., & Ajaymohan, R. S. (2010). Composite structure of monsoon low pressure systems and its relation to Indian rainfall. *Journal of Climate*, *23*, 4285–4305. https://doi.org/10.1175/2010JCLI2953.1

Krishnamurthy, V., & Shukla, J. (2007). Intraseasonal and seasonally persisting patterns of Indian monsoon rainfall. *Journal of Climate*, *20*, 3–20. https://doi.org/10.1175/JCLI3981.1

Lau, W. K. M., Kim, K. M., & Leung, L. R. (2017). Changing circulation structure and precipitation characteristics in Asian monsoon regions: Greenhouse warming vs. aerosol effects. *Geoscience Letters*, *4*, 28. https://doi.org/10.1186/s40562-017-0094-3

Li, X., Ting, M., Li, C., & Henderson, N. (2015). Mechanisms of Asian summer monsoon changes in response to anthropogenic forcing in CMIP5 models. *Journal of Climate*, *28*, 4107–4125. https://doi.org/10.1175/JCLI-D-14-00559.1

Lin, M., & Huybers, P. (2019). If rain falls in India and no one reports it, are historical trends in monsoon extremes biased? *Geophysical Research Letters*, *46*, 1681–1689. https://doi.org/10.1029/2018GL079709

Malik, N., Bookhagen, B., & Mucha, P. J. (2016). Spatiotemporal patterns and trends of Indian monsoonal rainfall extremes. *Geophysical Research Letters*, *43*, 1710–1717. https://doi.org/10.1002/2016GL067841

Mann, H. B. (1945). Nonparametric tests against trend. *Econometrica*, *13*, 245–259.

Mooley, D. A. (1973). Some aspects of Indian monsoon depressions and the associated rainfall. *Monthly Weather Review*, *101*, 271–280.

Mukherjee, S., Aadhar, S., Stone, D., & Mishra, V. (2018). Increase in extreme precipitation events under anthropogenic warming in India. *Weather and Climate Extremes*, *20*, 45–53. https://doi.org/10.1016/j.wace.2018.03.005

Pai, D. S., Sridhar, L., Badwaik, M. R., & Rajeevan, M. (2014). Analysis of the daily rainfall events over India using a new long period (1901–2010) high resolution (0.25° × 0.25°) gridded rainfall data set. *Climate Dynamics*, *45*(3–4), 755–776. https://doi.org/10.1007/s00382-014-2307-1

Pai, D. S., Sridhar, L., & Ramesh Kumar, M. R. (2016). Active and break events of Indian summer monsoon during 1901–2014. *Climate Dynamics*, *46*, 3921–3939. https://doi.org/10.1007/s00382-015-2813-9

Prajeesh, A. G., Ashok, K., & Rao, D. V. B. (2013). Falling monsoon depression frequency: A Gray–Sikka conditions perspective. *Scientific Reports*, *3*, 1–8. https://doi.org/10.1038/srep02989

Praveen, V., Sandeep, S., & Ajayamohan, R. S. (2015). On the relationship between mean monsoon precipitation and low pressure systems in climate model simulations. *Journal of Climate*, *28*, 5305–5324. https://doi.org/10.1175/JCLI-D-14-00415.1

Rajeevan, M., Bhate, J., & Jaswal, A. K. (2008). Correction to "Analysis of variability and trends of extreme rainfall events over India using 104 years of gridded daily rainfall data". *Geophysical Research Letters*, *35*, L18707. https://doi.org/10.1029/2008GL036105

Roxy, M. K., Ghosh, S., Pathak, A., Athulya, R., Mujumdar, M., Murtugudde, R., et al. (2017). A threefold rise in widespread extreme rain events over central India. *Nature Communications*, *8*(1), 708. https://doi.org/10.1038/s41467-017-00744-9

Roxy, M. K., Ritika, K., Terray, P., Murtugudde, R., Ashok, K., & Goswami, B. N. (2015). Drying of Indian subcontinent by rapid Indian Ocean warming and a weakening land–sea thermal gradient. *Nature Communications*, *6*, 7423. https://doi.org/10.1038/ncomms8423

Sandeep, S., Ajayamohan, R. S., Boos, W. R., Sabin, T. P., & Praveen, V. (2018). Decline and poleward shift in Indian summer monsoon synoptic activity in a warming climate. *Proceedings of the National Academy of Sciences of the United States of America*, *115*, 2681–2686. https://doi.org/10.1073/pnas.1709031115

Shastri, H., Paul, S., Ghosh, S., & Karmakar, S. (2015). Impacts of urbanization on Indian Summer Monsoon Rainfall extremes. *Journal of Geophysical Research: Atmospheres*, *120*, 496–516. https://doi.org/10.1002/2014JD022061

Sikka, D. R. (1977). Some aspects of the life history, structure and movement of monsoon depressions. *Pure and Applied Geophysics*, *115*, 1501–1529.

Singh, D. (2019). Implications of a varying observational network for accurately estimating recent climate trends. *Geophysical Research Letters*, *46*, 5430–5435. https://doi.org/10.1029/2019GL082330

Singh, D., Ghosh, S., Roxy, M. K., & McDermid, S. (2019). Indian summer monsoon: Extreme events, historical changes, and role of anthropogenic forcings. *Wiley Interdisciplinary Reviews Climate Change*, *10*, e571. https://doi.org/10.1002/wcc.571

Ullrich, P., & Zarzycki, C. (2017). Tempest Extremes: A framework for scale–insensitive pointwise feature tracking on unstructured grids. *Geoscientific Model Development*, *10*(3), 1069–1090. https://doi.org/10.5194/gmd-10-1069-2017

Vishnu, S., Boos, W. R., Ullrich, P. A., & O'Brien, T. A. (2020). Assessing historical variability of South Asian monsoon lows and depressions with an optimized tracking algorithm. *Journal of Geophysical Research: Atmospheres*, *125*, e2020JD032977. https://doi.org/10.1029/2020JD032977

Vishnu, S., Francis, P. A., Shenoi, S. S. C., & Ramakrishna, S. S. V. S. (2016). On the decreasing trend of the number of monsoon depressions in the Bay of Bengal. *Environmental Research Letters*, *11*(1), 014011. https://doi.org/10.1088/1748–9326/11/1/0140111

Yokoi, S., Takayabu, Y. N., & Murakami, H. (2013). Attribution of projected future changes in tropical cyclone passage frequency over the western North Pacific. *Journal of Climate*, *26*(12), 4096–4111. https://doi.org/10.1175/JCLI-D-12-00218.1

Yoon, J.-H., & Chen, T.-C. (2005). Water vapor budget of the Indian monsoon depression. *Tellus*, *57*, 770–782. https://doi.org/10.1111/j.1600-0870.2005.00145.x

You, Y., & Ting, M. (2021). Low pressure systems and extreme precipitation in Southeast and East Asian monsoon regions. *Journal of Climate*, *34*(3), 1147–1162. https://doi.org/10.1175/JCLI-D-20-0206.1

You, Y., Ting, M., & Camargo, J. S. (2021). *Heavy rain-producing terrestrial low-pressure systems over East Asian summer monsoon region: Evolution, energetics, and trend*. Journal of Climate, in press. https://doi.org/10.1175/JCLI-D-20-0667.1

Zarzycki, C. M., & Ullrich, P. A. (2017). Assessing sensitivities in algorithmic detection of tropical cyclones in climate data. *Geophysical Research Letters*, *44*, 1141–1149. https://doi.org/10.1002/2016GL071606

References From the Supporting Information

Bishop, D. A., Williams, A. P., & Seager, R., (2019). Increased fall precipitation in the southeastern United States driven by higher–intensity, frontal precipitation. *Geophysical Research Letters*, *46*, 8300–8309. https://doi.org/10.1029/2019gl083177

Roberts, M. J., Camp, J., Seddon, J., Vidale, P. L., Hodges, K., Vanniere, B., et al. (2020). Impact of model resolution on tropical cyclone simulation using the HighResMIP-PRIMAVERA multimodel ensemble. *Journal of Climate*, *33*(7), 2557–2583. https://doi.org/10.1175/JCLI-D-19-0639.1